ORIGINAL PAPER

Spatio-temporal characteristics of meteorological drought based on the MCI of Penman–Monteith

Haixia Yu[1,2] · **Dandan Yang**[1,2] · **Bingjun Liu**[1,2] · **Jianyu Fu**[1,2] · **Zhihao Liang**[1,2]

Abstract

The increasing global climate change has resulted in more frequent drought disasters, and using the drought index to assess spatial and temporal changes accurately is of practical importance. In this study, the Spatio-temporal evolution characteristics of different drought indicators at annual and seasonal scales were analyzed by combining spatial interpolation, correlation analysis, trend tests, and the empirical orthogonal function based on the meteorological drought composite index (MCI) of Penman–Monteith. The study focused on drought research in the Pearl River basin from 1961 to 2020. The results indicated that (1) on the annual scale, drought exhibited a high spatial distribution in the west and low in the east, as well as high in the south and low in the north. The frequency, intensity, and extent displayed a non-significant decreasing trend, with the drought degree being mild in the past ten years. (2) On the seasonal scale, drought exhibited seasonal variability, particularly in spring and autumn, which were inversely distributed. Summer drought was the least severe, with the drought range mostly below 10%, while winter drought was the severest, exceeding 50%, indicating an areawide drought. (3) The consistent change of drought intensity across the basin is the primary mode, and the reverse distribution of east–west and north–south is the secondary mode. The overall higher year of drought intensity is close to 24 years, and the overall lower year is close to 28 years. The study based on the MCI can provide a reference for drought research and management in different regions.

✉ Haixia Yu
    yuhaixia@mail.sysu.edu.cn

1   School of Civil Engineering, Sun Yat-Sen University, Guangzhou 510275,
    People's Republic of China

2   Key Laboratory of Water Cycle and Water Security, Southern China of Guangdong High
    Education Institute, Sun Yat-Sen University, Guangzhou 510275, People's Republic of China

1 Introduction

Under global warming, increasing extreme disasters pose threats to human health, economic growth, and the sustainability of both the natural and built environment (Wu et al. 2020; Zhou et al. 2021). Drought disasters, a type of extreme weather event, have affected nearly 2 billion people worldwide since the twentieth century and caused global economic losses of more than \$220 billion annually (Ma et al. 2021). Semi-arid and arid regions worldwide have been particularly affected by chronic water shortages and severe droughts in recent years, leading to crop failures and triggering great famines (Hao and Singh 2015; Chen et al. 2019). Since the 1950s, China has suffered from frequent and severe droughts, and the economic losses are estimated to reach 100 billion RMB (Qian et al. 2003; Liu et al. 2020). Therefore, studying the evolution of drought disasters is necessary, which aims to keep pace with rapid economic and social development.

Drought is a natural disaster characterized by prolonged water scarcity and is one of the natural disasters that cause significant losses and harmful effects on agricultural production and hydrological ecosystems. (Carrao et al. 2016; Schumacher et al. 2019; Li et al. 2020). According to the impacts on the hydrological ecosystem, society, and the environment, drought is mainly classified into four types, which are meteorological drought, hydrological drought, agricultural drought and socio-economic drought (Esfahanian et al. 2017; Seo et al. 2022). Among them, meteorological drought is typically the first type to manifest in drought occurrence (Zheng et al. 2022). The meteorological drought index plays a vital role in monitoring, predicting and assessing drought, serving as the basis of drought research (Greve and Seneviratne 2015). The PDSI (Palmer drought severity index), proposed in 1965, analyzes drought by calculating index values from precipitation and temperature factors, with limitations, such as fixed time scales (Palmer 1965; Wilhite 2017). In 1993, the SPI (Standardized precipitation index) was proposed, offering multi-timescale calculations that can characterize different stages of drought. This method has been widely applied (Mckee et al. 1993). The SPEI (Standardized precipitation evapotranspiration index) incorporates potential evapotranspiration based on the SPI, which retains the advantages of multiple time scales and takes into account the effect of temperature change on drought, making it a popular meteorological drought indicator (Vicente-Serrano et al. 2010). However, the SPI only considers precipitation, and the SPEI only adds temperature as an additional meteorological factor compared with the SPI. To enhance the accuracy of drought research, it would be beneficial to consider more factors (Huang et al. 2015). Moreover, crops in different regions and seasons exhibit varying degrees of sensitivity to soil moisture, and drought can show significant temporal and spatial variability through the water cycle and atmospheric circulation processes (Askari et al. 2017). Therefore, including a seasonal adjustment index in the calculation would lead to a more reasonable and accurate assessment of drought. The MCI (GB/T 20481-2017) can consider several meteorological factors, such as precipitation, temperature, and relative humidity at the same time. It has a unique seasonal adjustment coefficient, which can combine various meteorological factors and different seasonal crop water requirements to make a more accurate measurement and assessment of drought. While the MCI has been used to study drought in many regions of China (Han et al. 2021), it has not been applied and validated in the Pearl River basin, a classical coastal humid basin located in South China. It is thus feasible and necessary to use the MCI in the Pearl River basin further to analyze the drought risk.

In recent years, the drought issue in the Pearl River basin has gained significant attention. The increasing drought impacts have prompted numerous domestic and international

scholars to investigate the drought evolution in the Pearl River basin. Studies have revealed that the frequency, intensity and duration of extreme droughts in the Pearl River basin have increased since the 1970s, with autumn experiencing the most significant impact (Chen et al. 2016; Wang et al. 2018). In temporal terms, there is a trend of dry season wetting. Spatially, the western region shows a trend toward aridity, while the eastern and downstream regions show a trend toward increased moisture (Deng et al. 2018; Xu et al. 2019). Based on the SPEI, the duration of extreme annual droughts varies across different regions due to varying climatic influences (Xiao et al. 2016). Additionally, climate variability, runoff, and evapotranspiration significantly contribute to the dynamics of the drought process (Han et al. 2019). However, the majority of drought indices currently utilized in the Pearl River basin mainly take into account the precipitation and temperature, and present researches primarily focus on long-term scale (annual or seasonal scales). Therefore, the primary aim of this research is to introduce a new index for analyzing the long-term changes in the Basin at both annual and seasonal scales.

In this study, the MCI was used to investigate the spatial–temporal evolution of the drought in the Pearly River basin. The MCI was constructed based on the Penman–Monteith theory, which involves the effects of eight climatic factors, including precipitation, mean temperature, maximum temperature, minimum temperature, barometric pressure, relative humidity, wind speed, and insolation. In addition, seasonal adjustment coefficients were added to the investigation, which ensures full reflections of the actual drought conditions in the Pearl River basin. The spatial–temporal variations of the drought evolution at multiple scales were simultaneously explored using three indicators of drought days, intensity, and extent. The results provide a scientific reference for drought risk assessment, monitoring, and disaster prevention in the Pearl River basin. Moreover, our study could provide a new case and data support for global drought research and management forecasting.

2 Study region and data

2.1 Study region

The Pearl River basin, the second largest in China after the Yangtze River basin, comprises the Xijiang, Beijiang, and Dongjiang river systems, along with the Pearl River Delta system. These river systems flow from the west to the east, eventually reaching the southeast coast (Fig. 1) (Duan et al. 2021). The Pearl River basin experiences a tropical and subtropical climate with hot, humid, and wet weather, with annual precipitation averaging around 1,500 mm and average annual temperatures ranging between 14 and 22 °C (Chen et al. 2010; Lai et al. 2016; Li et al. 2020). Flow estimations indicate that approximately 80% of the basin's overall flow occurs during the flood season, which extends from April to September (Zhang et al. 2012). Despite rainfall having increased recently, the uneven spatio-temporal distribution of precipitation has resulted in frequent severe weather events, including drought disasters that have occurred almost every year since 2003, with significant droughts in 2009 and 2010. Continuous droughts have caused severe economic and social losses, in which the frequency of drought disasters accounts for about 1/5 of all natural disasters, and the reduction of grain production accounts for more than 5% of the overall production (Li et al. 2021; Wang et al. 2011). Given the Pearl River basin's strategic location and rapid urbanization, it is crucial to assess the spatial and temporal evolution of drought hazards at seasonal and annual scales. Such
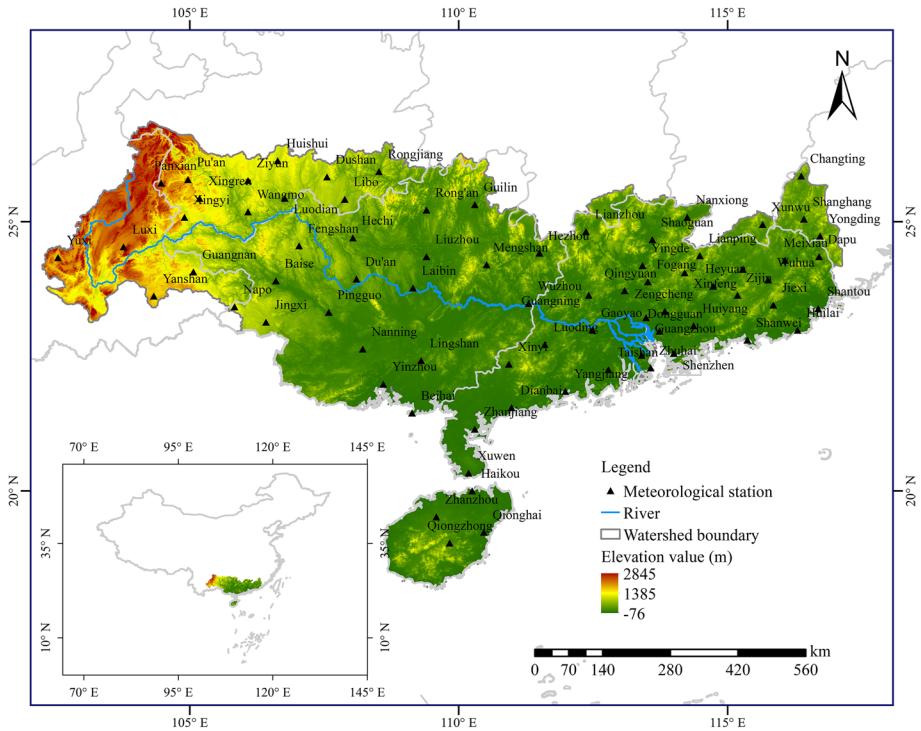
Fig. 1 Topographical map of the Pearl River basin

assessments provide a theoretical foundation for drought prevention and mitigation, facilitating local economic and social development.

2.2 Data

The meteorological data were obtained from the 'Daily Value Dataset of China's Terrestrial Climate Data (V3.0)' (http://data.cma.cn/dataService/). Meteorological data include precipitation, minimum temperature, maximum temperature, average temperature, atmospheric pressure, wind speed, sunshine hours and relative humidity in the Pearl River basin from 1961 to 2020. Rigorous quality checks have been conducted on the dataset by the National Meteorological Administration and the Meteorological Department. As a result, the meteorological data from the selected 75 stations have successfully passed integrity, reliability and consistency checks, ensuring the completeness and reliability for application in meteorological studies within the region (Wang et al. 2017; Yang et al. 2019).

3 Methodology

3.1 The meteorological drought composite index (MCI)

The MCI (GB/T 20481-2017) is a drought index that considers the influence of precipitation and evapotranspiration on current drought conditions during different periods in the preceding period. It incorporates the combined impact of effective precipitation (weighted cumulative precipitation) over 60 days, evapotranspiration (relative wetness) over 30 days, and precipitation on quarterly (90 days) and near half-yearly (150 days) scales. This index is particularly suitable for day-to-day monitoring (Eq. (1)). The drought classification categories of the MCI can be found in Table 1.

$$MCI = Ka \times \left(a \times SPIW_{60} + b \times MI_{30} + c \times SPI_{90} + d \times SPI_{150} \right) \tag{1}$$

$$MI = (P - PET)/PET \tag{2}$$

where $SPIW_{60}$ is the standardized weighted precipitation index for the last 60 days, MI_{30} is the relative wetness index for the previous 30 days, SPI_{90} is the standardized precipitation index for the previous 90 days, SPI_{150} is the standardized precipitation index for the previous 150 days P is precipitation and PET is the potential evapotranspiration for a given period, which is calculated by the FAO Penman–Monteith.

a, b, c, d are the weighting coefficients of each sub-item, *a* is 0.5, *b* is 0.6, *c* is 0.2, and *d* is 0.1 for the southern region of China, and *a* is 0.3, *b* is 0.5, *c* is 0.3 and *d* is 0.2 for the northern and western regions. The Pearl River basin is located in the southern part of China, *a* is 0.5, *b* is 0.6, *c* is 0.2, and *d* is 0.1.

The seasonal adjustment coefficient, *Ka*, is determined based on the sensitivity of the main crops to soil moisture at different stages of growth and development. It is generally assigned a value between 0.4 and 1.2. During the peak season (usually March to September), when crops require more water and are highly sensitive to soil moisture, a higher value of *Ka* (typically between 1.0 and 1.2) is used. Conversely, during the early growth or maturity period (usually October to February), when crops require less water and are less sensitive to soil moisture, a lower value of *Ka* (generally between 0.4 and 1.0) is applied. This study uses Rongjiang, Libo, and Guangnan as dividing lines, with *Ka*-1 located to the west and *Ka*-2 to the east (Table 2).

Table 1 Drought classification standard of the MCI

Level	MCI value	Drought classification
1	$-0.5 < MCI$	Normal
2	$-1.0 < MCI \le -0.5$	Light drought
3	$-1.5 < MCI \le -1.0$	Moderate drought
4	$-2.0 < MCI \le -1.5$	Severe drought
5	$MCI \le -2.0$	Extreme drought

Table 2 Seasonal adjustment coefficient in different months	Month	1	2	3	4	5	6	7	8	9	10	11	12
	Ka-1	1.0	1.0	1.1	1.2	1.0	1.2	1.2	1.2	1.0	1.0	1.0	1.0
	Ka-2	0.9	0.9	1.0	1.0	1.2	1.2	1.2	1.2	1.0	1.0	0.9	0.9

3.2 Drought assessment indicator

The number of drought days, the cumulative intensity, the ratio of drought stations, and the extent of drought impact are selected as indicators for drought assessment, and each hand is calculated as follows.

Drought days: The "Drought days" refers to the total count of days where the daily MCI value is less than or equal to -1.

Cumulative drought intensity: It is calculated by summing the absolute values of the daily MCI for droughts categorized as above light drought. A higher cumulative value indicates a more significant drought intensity, while a lower one suggests a lower one.

Drought Station Ratio: It is determined by dividing the number of drought-affected stations in a region by the total number of stations in that region. This ratio helps assess the extent of drought impact.

Drought-affected area: The magnitude of the drought station ratio within the basin serves as an indicator of drought extent, providing insights into the affected area and the severity of the drought. If $P_i < 10\%$, it's no apparent drought. If $10\% \leq P_i < 25\%$, localized drought; if $25\% \leq P_i < 33\%$, partial regional drought; if $33\% \leq P_i < 50\%$, regional drought; if $P_i = 50\%$, area-awide drought.

$$P_i = \frac{N_i}{N} \times 100\% \tag{3}$$

3.3 Statistical analysis

3.3.1 Correlation analysis

This study employed the Person, Spearman, and Kendall correlation coefficient methods to examine the correlation among drought indicators at various scales. A stronger correlation is indicated when the index value tends to approach 1.

3.3.2 Trend analysis

Apart from using the linear trend method to analyze drought indicators, the Mann-Kendall test was employed for trend and mutation testing (Mann 1945; Kendall 1990). The MK test can be applied for trend-testing time series encompassing drought days, cumulative drought intensity, and drought station ratio.

Construct an order column for a given time series x.

$$S_k = \sum_{i=1}^{k} r_i \tag{4}$$

$$r_i = \begin{cases} +1, & \text{if } x_i > x_j \\ 0, & \text{else} \end{cases} \quad (j = 1, 2, \dots, i) \tag{5}$$

Each statistic for a random variable time series is calculated using the following equation.

$$UF_k = \frac{S_k - E(S_k)}{\sqrt{\text{Var}(S_k)}} \quad (k = 1, 2, \dots, n) \tag{6}$$

$$E(s_k) = \frac{n(n-1)}{4} \tag{7}$$

$$\text{Var}(s_k) = \frac{n(n-1)(2n+5)}{72} \tag{8}$$

$$UB_k = -UF_k \tag{9}$$

Giving a significance level α, check the standard distribution table, if $|UF_i| > U_\alpha$, it means that there is a significant trend. When the value of UF_k is greater than 0, it indicates that it is on an upward trend, and less than 0 shows a downward trend. The time corresponding to the intersection of the two curves of UF_k and UB_k can be determined as the time when the mutation starts. The chosen significance level $\alpha = 0.05$ and a check of the table gives $U_{0.05} = \pm 1.96$.

3.4 Empirical orthogonal function

The EOF, introduced by Lorenz into meteorology and climate research, is a technique for extracting key data features by examining the structural properties of matrix data (Xu and Kamide 2004) (Pei et al. 2015). In this study, the EOF is employed to derive the geographical vector matrix and the temporal coefficient matrix from the matrix of drought cumulative intensity. The typical spatial distribution patterns and trend characteristics of the temporal coefficients are identified by assessing the magnitude of variance contribution. Furthermore, the analysis includes examining spatial anomaly characteristics and temporal variation patterns.

Select the cumulative intensity to be analyzed, show the data in matrix form, and perform anomaly processing on matrix X.

$$X_{m \times n} = \begin{pmatrix} x_{11} & x_{12} & \cdots & x_{1n} \\ x_{21} & x_{22} & \cdots & x_{2n} \\ \cdots & \cdots & \cdots & \cdots \\ x_{m1} & x_{m2} & \cdots & x_{mn} \end{pmatrix} \tag{10}$$

The variable $X_{m \times n}$, consisting of n observations and m spatial points is viewed as a linear combination of p spatial feature vectors and the corresponding temporal weighting coefficients.

$$X_{m \times n} = V_{m \times p} T_{p \times n} \tag{11}$$

V is the spatial eigenvector and T is the time factor. This process concentrates the main information of the climatic variable field into a few typical eigenvectors.

4 Results

4.1 Seasonal variation of drought days

The Pearl River basin consistently experiences the highest drought days during winter, followed by spring and autumn, and the lowest during summer. The regional distribution has a clear seasonal pattern, exhibiting an east–west and south-north reverse gradient. Additionally, there is a distinct spatial reverse gradient during spring and autumn.

Trend analysis on the seasonal scale of the drought days series shows a flat trend per year in summer, a very slight increasing trend in autumn, and a decreasing trend in spring and winter (Fig. 2). The drought days in summer increase with a movement of 0.002/a and drought conditions are stable, mainly because of the abundant summer rainfall and the relatively wet conditions throughout the basin. The number of drought days increases in autumn with a trend of 0.05/a, while it decreases in spring and winter with a movement of 0.11/a and 0.21/a, respectively. Various factors have contributed to slight variations in meteorological factors such as precipitation and temperature, particularly in spring, autumn, and winter. The number of drought days shows an increasing trend of 0.05/a in autumn, while it decreases in spring and winter with trends of 0.11/a and 0.21/a, respectively. Slight variations in meteorological factors, including precipitation and temperature, have been observed in spring, autumn, and winter, influenced by various factors.

The distribution of drought days is high in the west and low in the east, as well as high in the south and low in the north in spring and winter. In autumn, the distribution is just
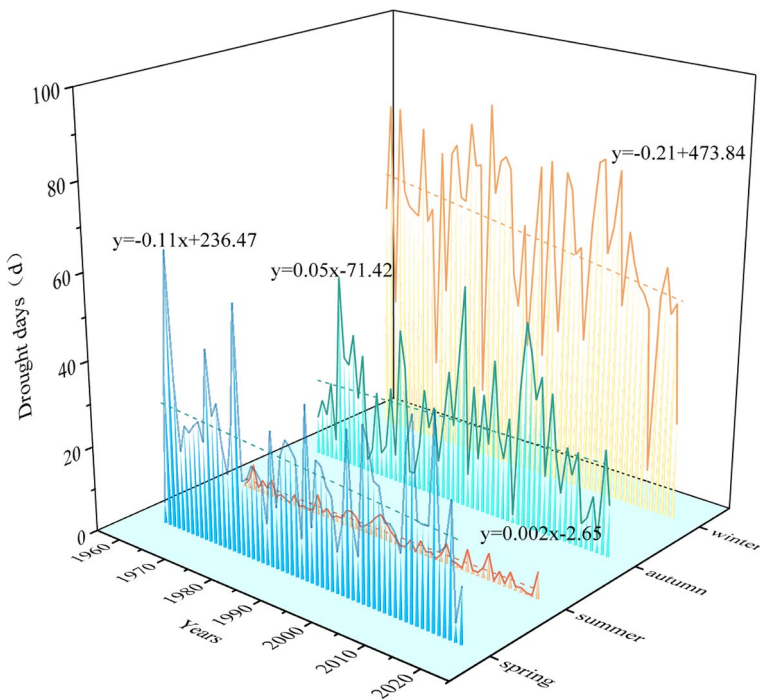

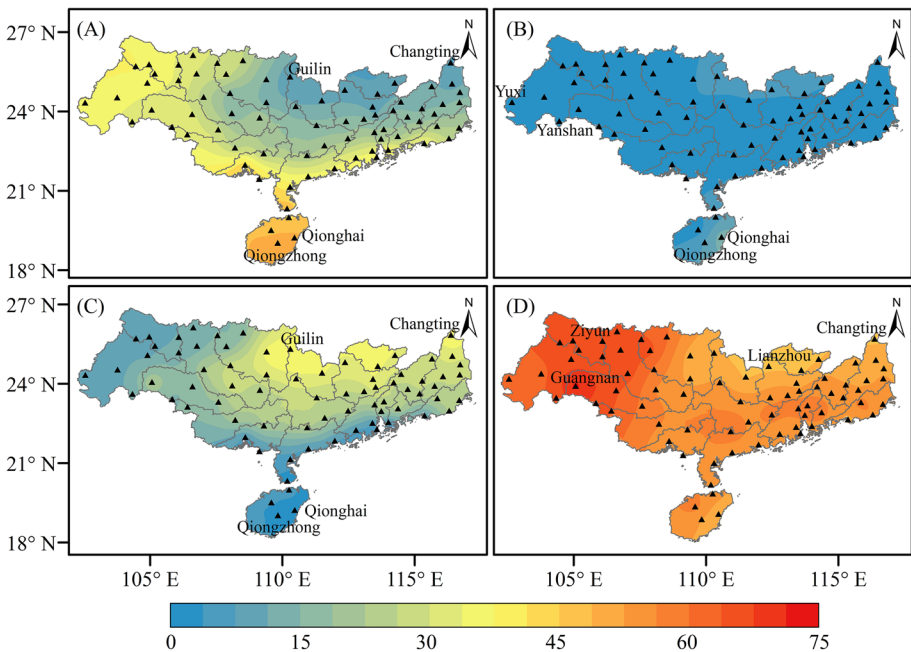**Fig. 2** The time series of seasonal drought days

the opposite (Fig. 3). On the other hand, there are relatively few drought days throughout the basin in summer. Figure 2 highlights the stations with the highest and lowest drought days. Among these stations, Qionghai, Qiongzhong, and Changting occur most frequently. However, they do not consistently have the highest or lowest values of drought days. This means that areas with relatively high dry days in one season may have lower values of dry days in the following season.
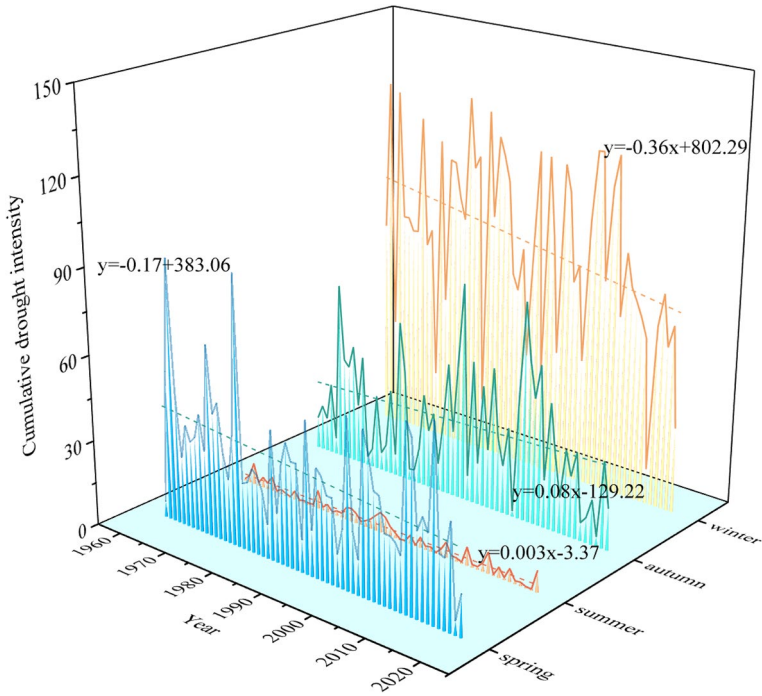
4.2 Seasonal variation of cumulative drought intensity

The distribution of high and low drought intensity zones exhibits seasonal variability and is not constant throughout the seasons. The cumulative intensity values are most significant in winter, followed by spring and autumn, and least in summer. There is a consistent east–west and north–south reversal across the basin. Similarly, spring and autumn also exhibit a reversed spatial distribution pattern.

The drought intensity values exhibit a decreasing tendency of 0.17/a and 0.36/a in spring and winter, an increase of 0.08/a in autumn, and show slight yearly variation in summer (Fig. 4). The southern Hainan region exhibits high values in spring, while the central and northeastern basins have low values. Autumn and spring show an opposite pattern, with high values in one region and low values in the other (Fig. 5). In winter, the western basin experiences high values, while the southern, central, and northeastern regions have low values. Overall, there is a strong resemblance between the cumulative drought intensity and the drought days in both the spatial characteristics across seasons and the temporal variation over time.
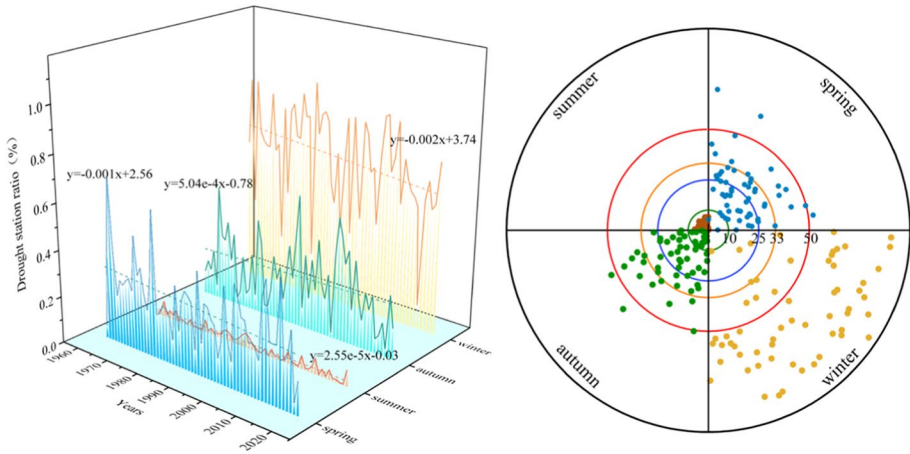

Fig. 3 The spatial distribution of seasonal drought days (**A**-spring, **B**-summer, **C**-autumn, and **D**-winter)
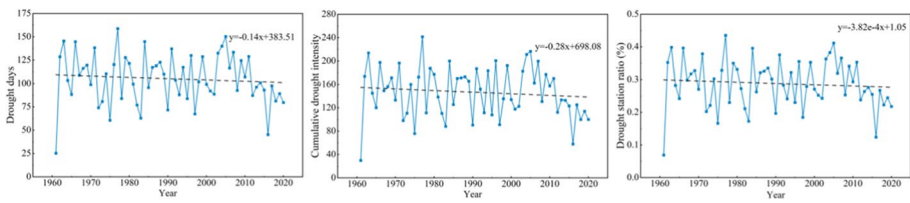
Fig. 4 The time series of seasonal cumulative drought intensity
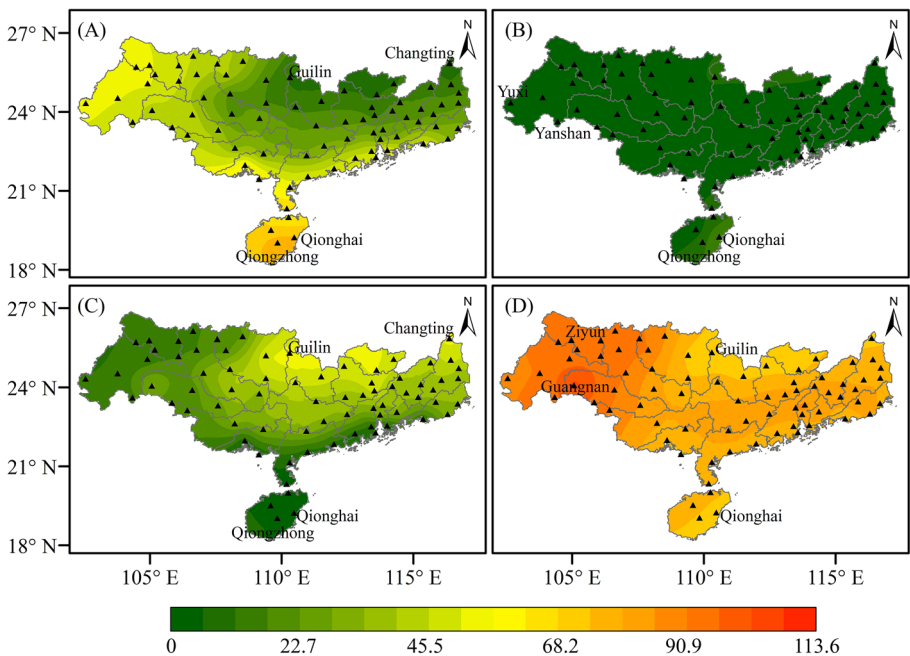
Fig. 5 The spatial distribution of seasonal cumulative drought intensity (**A**-spring, **B**-summer, **C**-autumn, **D**-winter)

Fig. 6 Seasonal variation of drought station ratio

Fig. 7 Time series of annual average indicators

4.3 Seasonal variation of drought station ratio

Regarding the drought extent, the drought station ratio exhibits significant fluctuations across the seasons. Overall, the drought-affected area: winter > spring > autumn > summer, with a decreasing trend in all seasons except for autumn (Fig. 6). For the type of drought extent, over the past 60 years, winter has been chiefly an areawide drought at 83%, spring and autumn have mainly been regional droughts, and summer is all within no apparent drought (Fig. 7).

In the majority of years, spring drought impact ranges between 10 and 25%, followed by 25–33%, for a total of 70%. All summers observe between 0 and 10%. The vast majority of autumn years keep between 10 and 25%, followed by 0–10%, for a total of 63%. As for winter, there have been 50 years with drought station ratios exceeding 50%. Thus, from the impact range interval, it can be inferred that spring is primarily characterized by localized and part of the regional drought. Summer, on the contrary, generally experiences no apparent drought. Autumn exhibits localized or no apparent drought. Lastly, winter is predominantly associated with areawide drought.

4.4 Temporal changes in annual drought

The annual time series of the three indicators exhibit similar decreasing trends, with drought intensity showing a more substantial decline compared to drought days and station ratio. However, the decreasing tendencies for all three indicators are not significant. The average drought indicator fluctuated up and down more steadily over the first forty years, with consistently high values in the early decade of the twentieth century, before beginning to decrease in the last decade and reaching its lowest value in 2016. Analysis of mutability and trends shows that the years 1963, 1977 and 2005 were severe years of drought.

Regarding the variation in annual drought days (Fig. 7), the highest number of drought days is in 1977, followed by 2005, 1963, and 2004, and the periods of sustained 3-year drought days were 1961–1963, 2003–2005, and 2008–2010. Annual drought days were significantly higher in the early twentieth century but tended to decline rapidly after the 2010s. In terms of cumulative annual drought intensity changes, the highest recorded was observed in 1977, followed by 2005, 1963 and 1964. 1986–1988, 2003–2005 and 2006–2008 were periods of consistently strong mean annual drought intensity values, with a subsequent decline after the 2010s. The change in the average annual drought station ratio shows a smooth trend with no apparent upward or downward trend. Since 1961, the highest average yearly drought station ratio was observed in 1977 at 0.43, followed by 2005, 1963, and 1966. The weakest ratio in the last 60 years was recorded in 2016 at 0.12.

The Mann-Kendall test was conducted on annual drought days, annual drought cumulative intensity and annual drought station ratio (Fig. 8), which showed that the time series of these variables exhibited stable characteristics and overall stable fluctuations, with no significant mutation years or notable changes. Specifically, there is no significant abrupt change or significant trend in 1961–2000. 2000–2010, a slight upward trend was observed, although it was not statistically significant. Subsequently, from 2010 to 2020, a non-significant downward trend was observed.
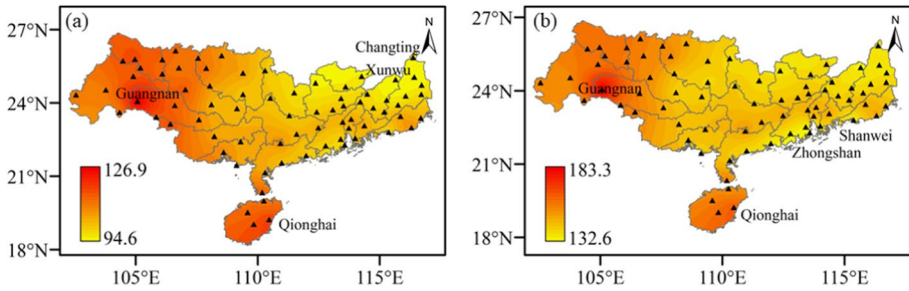
4.5 Spatial distribution in annual droughts

The spatial pattern of annual drought days and cumulative intensity exhibits a general consistency, with high correlation coefficients reaching up to 0.95. The areas with high frequencies of drought days align closely with the centers of high intensity, especially in the basin's west and Hainan Island region.

The perennial value of annual dry days (Fig. 9a) is generally 94.6–126.9 d in most of the central basin, with many locations in the southern and western regions exceeding 115 d, reaching a maximum of 126.9 d at Guangnan. In the eastern region, the days are usually below 100 d, with the lowest value observed in Changting and Xunwu, not exceeding 95 d.
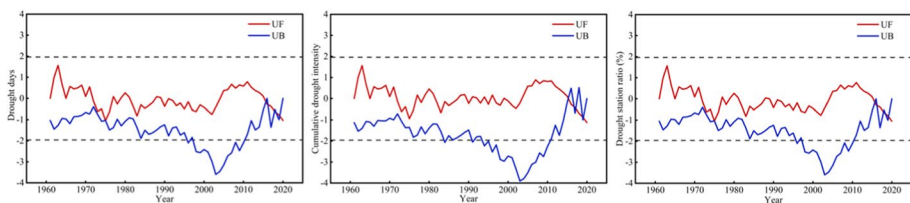
**Fig. 8** MK test for each indicator of the annual scale

Fig. 9 The spatial distribution of annual average indicators

The annual cumulative drought intensity (Fig. 9b) shows an increasing trend in the northeast-to-southwest direction, with two high centers, one located around Guangnan with intensity values up to 183.3, and the other around Hainan Island, with the highest value at Qionghai, reaching 164.2. The lowest intensity value is found in the Zhongshan and Shanwei along the southeast coast, averaging around 133.

4.6 Correlation analysis of drought indicators

After evaluating the spatial evolution characteristics of the drought days, cumulative drought intensity, and drought station ratio at both annual and seasonal scales, it is observed that the three drought indicators exhibit similar spatial distributions. In this regard, correlation analyses were conducted for annual (Fig. 10) and seasonal scales (Table 3), including Person, Spearman, and Kendall correlation methods.

The results indicate a strong correlation between drought cumulative intensity, drought days, and drought station ratio, with correlation coefficients exceeding 0.9 for both seasonal and annual scales, it means that the analysis of drought cumulative intensity can provide insights into the current situation of drought days and drought station ratio to a certain extent. Therefore, for the subsequent spatial–temporal decomposition analysis of drought, the EOF was chosen for decomposing the spatial and temporal patterns of cumulative intensity.
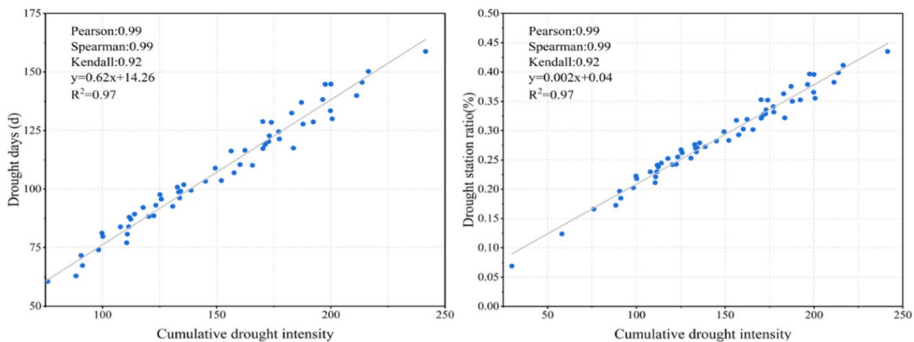
Fig. 10 Correlation analysis of annual drought indicators

Table 3 Correlation analysis of seasonal drought indicators

Season	Drought days and intensity				Drought intensity and station ratio			
	Spring	Summer	Autumn	Winter	Spring	Summer	Autumn	Winter
Pearson	0.98778	0.9981	0.99261	0.98198	0.98778	0.9981	0.99261	0.93879
Spearman	0.98893	0.99918	0.99617	0.97942	0.98893	0.99914	0.99617	0.94159
Kendall	0.93077	0.98727	0.96723	0.89686	0.93077	0.98643	0.96723	0.85424

4.7 Spatio-temporal decomposition of cumulative drought intensity using EOF

4.7.1 Modal variance contribution

The matrix of the cumulative drought intensity at annual and seasonal scales was subjected to the EOF decomposition (Table 4). The results show that the first two modes of annual and each season are the primary modes, providing a more comprehensive drought intensity and capturing most information on the spatio-temporal decomposition. The variance contributions of the first two modes were substantial, accounting for 78% in the interannual scale, 76% in spring, 53% in summer, 80% in autumn, and 84% in winter. The first two modes significantly contribute to the cumulative variance, with non-overlapping error ranges and passing the North significance test. Modes beyond the third mode exhibit relatively small contributions and can be disregarded.

Table 4 Variance contribution of the first three modes of EOF

Time	Modal	Variance contribution	accumulated variances contribution	Characteristic root error	
				lower limit	upper limit
Year	1st	0.65	0.65	115,742.56	160,921.63
	2nd	0.13	0.78	23,422.60	32,565.40
	3rd	0.07	0.85	14,045.63	19,528.22
Spring	1st	0.59	0.59	22,269.06	30,961.58
	2nd	0.17	0.76	6623.68	9209.18
	3rd	0.08	0.84	3286.79	4569.76
Summer	1st	0.35	0.35	624.42	868.16
	2nd	0.18	0.53	323.46	449.72
	3rd	0.07	0.60	153.33	213.18
Autumn	1st	0.66	0.66	26,284.39	36,544.27
	2nd	0.14	0.80	5376.63	7475.34
	3rd	0.04	0.84	1668.09	2319.22
Winter	1st	0.69	0.69	55,283.24	76,862.56
	2nd	0.14	0.84	11,871.55	16,505.50
	3rd	0.06	0.90	4813.21	6691.99

4.7.2 Analysis of the spatial and temporal decomposition in seasonal droughts

Figure 11 illustrates the spatial pattern of coefficients and their corresponding temporal variations for each season's first and second modes. The first mode serves as the main control mode, reflecting a consistent variation pattern of drought intensity, while the second mode reflects two distinct spatial distributions for each season, an east–west reverse distribution and a north–south reverse distribution. There is a trend towards alleviated drought conditions in winter and spring, an increasing tendency in autumn, and relatively stable drought intensity during summer. Notably, 1963, 1977, 2014, and 1979 represent typical years of drought in four seasons, respectively.

The regions near Beihai station, Qionghai station, Yingde station, and Huiyang station exhibit high values in the four seasons, serving as the primary control areas for the first mode. Specifically, the southern area near Beihai, the south region near Qionghai, the northern area near Yingde, and the western area near Huiyang are relatively sensitive to drought changes in all seasons. According to the temporal coefficients, it is observed that the coefficient for spring displays a decreasing trend of 1.4958/a, indicating a direction of drought alleviation in spring. Conversely, there is minimal change in summer, an increasing tendency in autumn, and a tendency for drought relief in winter.

The second mode reflects the secondary distribution pattern in each season. In spring, Guilin, Liuzhou, Du'an, and Pingguo act as dividing lines. The mode shows a negative trend to the west of these dividing lines and a positive trend to the east. This indicates an east–west reversal with Guilin Station and Pingguo as the boundaries. Similarly, there is a north–south reversal in summer with Zhanjiang as the boundary. In autumn, an east–west reversal is observed with Hezhou, Laibin, and Baise as the boundaries. There is an east–west reversal in winter with Hezhou, Mengshan, and Lingshan as the boundaries. Analyzing the temporal coefficients for the second mode in the four seasons, it can be observed that drought intensity increases in the eastern region during spring. In summer, drought intensity remains relatively unchanged across the basin. In
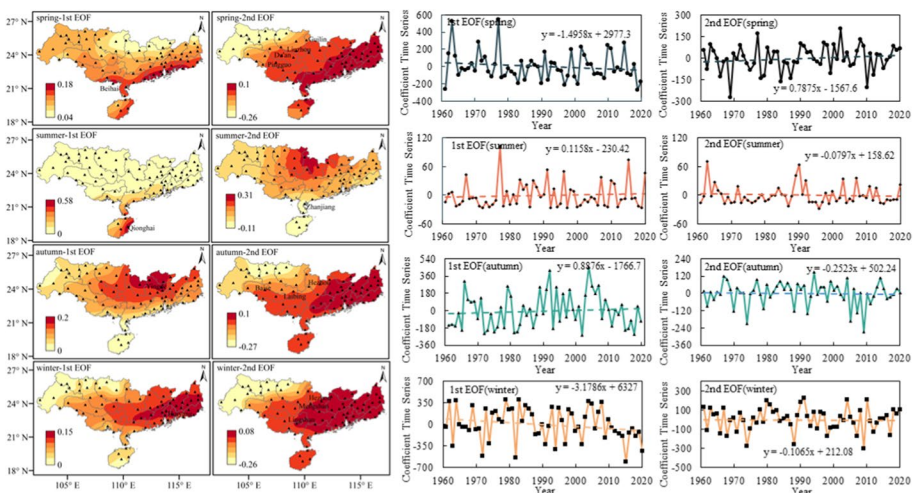

Fig. 11 Spatial and temporal decomposition of EOF for seasonal-scale cumulative intensity

autumn, there is relief in the eastern region, while the intensity increases in the western part. Winter and autumn exhibit a relatively consistent pattern.

4.7.3 Analysis of the spatial and temporal decomposition in annual droughts

The spatial and temporal coefficients of the first two modes, obtained by decomposing the annual cumulative drought intensity into time and space, are depicted in Fig. 12. The analysis shows a consistency in the variation of annual drought intensity reflected in the main modes across the basin, with 1963, 1977, 2004, and 2005 being typical years. Overall there is a year-on-year easing trend, especially in the last decade when the basin has been in stable and low levels of drought. From 1961–2020, the basin encountered 24 years of high-intensity drought, 28 years of low-intensity drought, 4 years of low intensity in the southeast and high in the northwest, and 4 years of high intensity in the southeast and low in the northwest.

The spatial coefficients for the first mode exhibit positive values, indicating a consistent pattern of annual drought intensity variation. Specifically, 1977, 2004, 2005 and 1963 have the highest time coefficients and serve as typical examples of annual droughts. On the other hand, the spatial coefficient of the second mode shows an opposite distribution from east to west, with negative values in the east and positive values in the west, delineated by the boundary line of Rong'an, Fengshan, and Guangnan. The temporal coefficient for the second mode displays an increasing trend of 0.2287/a. Consequently, the drought intensity in the northwestern part, defined by the boundary line of Rong'an, Fengshan, and Guangnan, tends to intensify, while the southeastern part experiences a tendency towards alleviation.

Over the past 60 years, four distinct spatial patterns of drought intensity have been identified: high intensity throughout the entire basin, low intensity throughout the entire basin, high intensity in the northwest and low in the southeast, and low intensity in the northwest and high in the southeast. For each year, the modal drought spatial distribution was determined by selecting the eigenvector with the highest absolute value of the time coefficient.
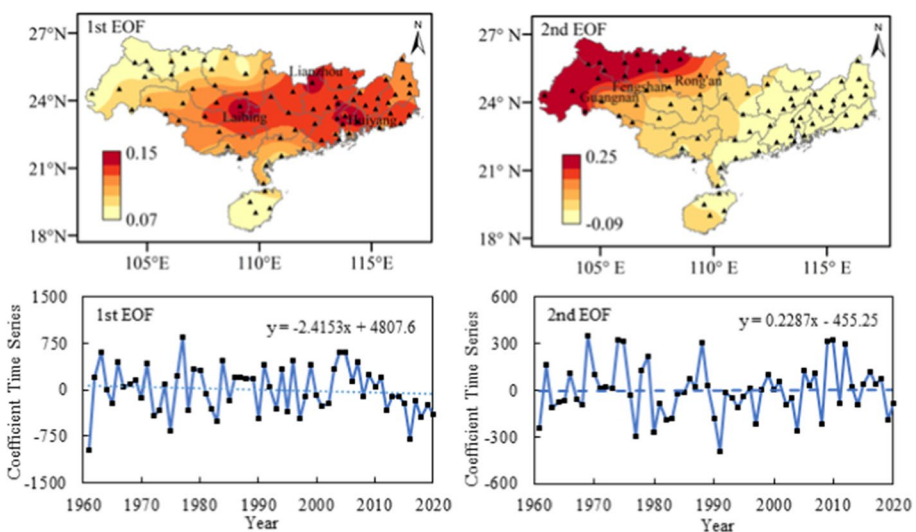

Fig. 12 Spatial and temporal decomposition of EOF for annual-scale cumulative intensity

This analysis revealed 24 years of high basin-wide drought intensity, 28 years of low basin-wide drought intensity, 4 years of high intensity in the northwest and low in the southeast, and 4 years of low intensity in the northwest and high in the southeast (Fig. 13). The distribution pattern of cumulative drought intensity over the 54 years was predominantly characterized by the first mode, accounting for 90% of the total years. This highlights that the basin-wide drought distribution represented by the first mode remains consistent and is the dominant form of drought distribution.

5 Discussion

On an annual scale, the western and southern areas of Hainan Island experienced more severe drought conditions in the Pearl River basin, with the indicators of drought days, intensity, and extent decreasing over the 60 years, indicating an overall trend of drought relief. At the seasonal scale, drought exhibited variations among seasons, with the order of drought intensity being winter > spring > autumn > summer, and only autumn showing an increasing trend in drought intensity. Previous studies have also reported similar findings, indicating that the MCI index can effectively identify and assess drought characteristics comparable to other widely used indices (Chen 2020; Fang 2020). Furthermore, the spatial distribution of drought varies across seasons, with most areas experiencing aridity in spring and autumn, while the study area predominantly exhibits wetting trends in summer and winter (Huang et al. 2010; Jing et al. 2021; Xie et al. 2020). These findings align with this study's results, highlighting the MCI index's ability to capture and assess seasonal drought patterns.

Additionally, the analysis conducted in this study revealed some specific phenomena regarding seasonal drought. Firstly, there is a reversed spatial distribution of droughts between spring and autumn. Secondly, the areas with high drought severity in spring correspond to those with low drought severity in autumn, and vice versa. This pattern coincides with the shift in monsoon circulation during the autumn season in the Pearl River basin. As the South China Sea monsoon weakens, it still brings some precipitation to southern areas like Hainan Island, alleviating drought conditions. Conversely, regions such as Guilin and Changting in the south of the basin experience more severe droughts as precipitation decreases due to the weakening and reversal of the East Asian monsoon (Fan et al. 2013; Huang et al. 2017). This interesting phenomenon is closely related to monsoonal and atmospheric circulation patterns, tropical cyclone movements, greenhouse gas emissions and topographic features during different seasons (Ostad-Ali-Askari 2022a).

Typical drought years on the seasonal time scales include 1963 for spring, 1977 for summer, 2004 for autumn, and 1979 for winter. On the annual time scale, the typical drought years are 1963, 1977, 2004, and 2005. These findings indicate that the drought in
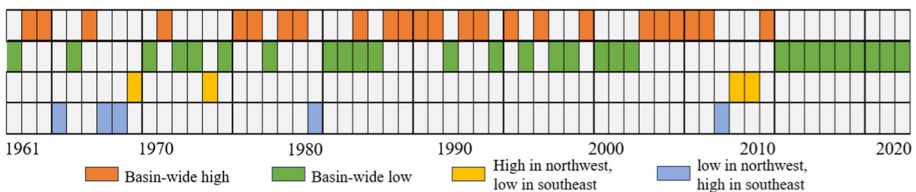

Fig. 13 Spatial distribution of droughts in the main modes per year

spring was mainly attributed to the extent of the annual drought in 1963, while the drought in 1977 was predominantly a summer drought, and the drought in 2004 was primarily an autumn drought. The drought in 1979 was a combination of droughts occurring in all seasons. It has been observed that the Pearl River basin has experienced anomalous cumulative precipitation, with a decreasing trend in two periods: 1984–1992 and 2003–2011 (Huang et al. 2021). The basin's main years characterized by severe drought include 1963, 1999, and 2003, with 1963 being the most severe, extensive, and prolonged drought, persisting for almost the entire year (Li et al. 2021; Huang et al. 2019; Jing et al. 2020;). While different drought research methods and indicators may yield slightly different results regarding the specific years of drought, the mega-drought in 1963 and the drought conditions from 1977 to 1979 and 2003 to 2004 in the basin warrant further analysis.

A spatial and temporal decomposition analysis was conducted for typical droughts, revealing 24 years of high drought intensity across the basin over the past 60 years, as well as 4 years of high drought intensity in the northwest and 4 years of high drought intensity in the southeast. Therefore, drought prevention and management strategies should be tailored to each season and specific sub-regions within the basin. Future efforts could explore implementing hydraulic facilities and various irrigation methods, such as furrow irrigation and border irrigation, in water management settings of different regions (Ostad-Ali-Askari 2022b; Javadi et al. 2023). Furthermore, with the abrupt changes in global climate and increased carbon emissions from industrial development, the greenhouse effect and climate change have intensified, impacting the occurrence and severity of droughts. Regions experiencing severe drought are particularly vulnerable to forest fires (Javadinejad et al. 2019; Rabiei et al. 2022). Given the superior natural ecological environment of the Pearl River basin, ecological fire prevention becomes even more crucial. Analyzing the intrinsic relationship between drought indices and fire risk factors holds significant importance for the survival and development of the basin.

6 Conclusion

This paper investigates the distribution characteristics of drought frequency, extent and intensity in the Pearl River basin from 1961 to 2020 and their interrelationships based on the MCI, using correlation analysis, trend analysis and the EOF method.

The study found that (1) there was a slight relief in drought across the basin from year to year, with 24 years of high drought intensity, 28 years of low drought intensity, 4 years of high drought intensity in the northwest, and 4 years of high drought intensity in the southeast over a period of 60 years. Over the past decade, there has been a gradual reduction in drought intensity, leading to stable drought conditions throughout the basin, reaching its lowest level in 2016. (2) Drought is more significant in winter than in spring and autumn than in summer, and it eases in all seasons except autumn when there is a tendency for drought to intensify. (3) Spatially, drought days and intensity distribution are consistent on both seasonal and annual scales. Areas of high drought intensity are basically located in the western and southern regions of the basin in the Hainan Island region, with drought intensity showing a distribution of high west and low east, and high south and low north in spring and winter, low drought intensity across the basin in summer, and a distribution of high east and low west and high north and low south in autumn. (4) A rather peculiar point is that the spring and autumn drought distributions are characterized by an inverse

distribution, with the high-value areas of drought intensity in spring being the low-value areas in autumn and the low-value areas in spring being the high-value areas in autumn.

These findings are of great scientific significance for drought risk assessment, monitoring and disaster prevention and mitigation in the Pearl River basin, and provide new cases and data support for global drought research. At the same time, this paper's research methods and findings also provide a reference for drought research in other regions and provide a scientific basis for addressing global climate change and drought management predictions.

Declarations

Competing interests The authors have not disclosed any competing interests.

References

Askari KOA, Shayannejad M, Eslamian S (2017) Deficit irrigation: optimization models. In: Handbook of drought and water scarcity, vol. 3: management of drought and water scarcity. CRC Press, Boca Raton

Carrao H, Naumann G, Barbosa P (2016) Mapping global patterns of drought risk: an empirical framework based on sub-national estimates of hazard, exposure and vulnerability. Glob Environ Change-Hum Policy Dimens 39:108–124

Chen S, Gan TY, Tan X et al (2019) Assessment of CFSR, ERA-Interim, JRA-55, MERRA-2, NCEP-2 reanalysis data for drought analysis over China. Clim Dyn 53:737–757

Chen YD, Zhang Q, Xiao M et al (2016) Probabilistic forecasting of seasonal droughts in the Pearl River basin, China. Stoch Environ Res Risk Assess 30:2031–2040

Chen YD, Zhang Q, Xu C-Y et al (2010) Multiscale streamflow variations of the Pearl River basin and possible implications for the water resource management within the Pearl River Delta, China. Quat Int 226:44–53

Chen Z (2020) Empirical diagnostic analysis on spatial and temporal variations of droughts in the Pearl River basin, China. Acta Scientiarum Naturalium Universitatis Sunyatseni 59:33–42

Deng S, Chen T, Yang N et al (2018) Spatial and temporal distribution of rainfall and drought characteristics across the Pearl River basin. Sci Total Environ 619:28–41

Duan R, Huang G, Li Y et al (2021) Stepwise clustering future meteorological drought projection and multi-level factorial analysis under climate change: a case study of the Pearl River Basin. China Environ Res 196:110368

Esfahanian E, Nejadhashemi AP, Abouali M et al (2017) Development and evaluation of a comprehensive drought index. J Environ Manage 185:31–43

Fan L, Zhang F, Hu Z et al (2013) Spatial and temporal features of dry and wet states in South China in recent 50 years. Trans Atmos Sci 36:29–36

Fang W (2020) Assessing time-varying risk of drought and flood from a multivariate perspective in the Pearl River Basin, China. Doctor, Xi'an University of Technology

Greve P, Seneviratne SI (2015) Assessment of future changes in water availability and aridity. Geophys Res Lett 42:5493–5499

Han L, Zhang Q, Zhang Z et al (2021) Drought area, intensity and frequency changes in China under climate warming, 1961–2014. J Arid Environ 193:104596

Han Z, Huang S, Huang Q et al (2019) Propagation dynamics from meteorological to groundwater drought and their possible influence factors. J Hydrol 578:124102

Hao Z, Singh VP (2015) Drought characterization from a multivariate perspective: a review. J Hydrol 527:668–678

Huang W, Yang X, Li M et al (2010) Evolution characteristics of seasonal drought in the south of China during the past 58 years based on standardized precipitation index. Trans Chin Soc Agric Eng 26:50–59

Huang S, Chang J, Leng G, Huang Q (2015) Integrated index for drought assessment based on variable fuzzy set theory: a case study in the Yellow River basin, China. J Hydrol 527:608–618

Huang C, Zhang Q, Chen X et al (2017) Spatio-temporal variations of dryness/wetness and influence from climate factors in Pearl River basin. J China Hydrol 37:12-20

Huang Q, Cheng Z, Tang C et al (2019) Monitoring the spatio-temporal process of severe droughts in the Pearl River basin. Adv Earth Sci 34:1050–1059

Huang Z, Jiao JJ, Luo X et al (2021) Drought and flood characterization and connection to climate variability in the Pearl River basin in southern China using long-term grace and reanalysis data. J Clim 34:2053–2078

Javadi A, Ostad-Ali-Askari K, Talebmorad H (2023) Effect of simultaneous variations of Kostiakov–Lewis infiltration coefficients equation in irrigation management on SIRMOD model outputs. Arab J Geosci 16:289

Javadinejad S, Eslamian S, Ostad-Ali-Askari K (2019) Investigation of monthly and seasonal changes of methane gas with respect to climate change using satellite data. Appl Water Sci 9:180

Jing W, Zhao X, Yao L et al (2020) Can terrestrial water storage dynamics be estimated from climate anomalies? Earth Space Sci 7:e2019EA 000959

Jing J, Xu Y, Wang Y et al (2021) Characteristics of multi-scale drought and flood in the Pearl River Basin from 1960 to 2019. Res Agric Mod 42:557–569

Kendall MG (1990) Rank correlation methods. Br J Psychol 25:86–91

Lai C, Chen X, Wang Z et al (2016) Spatio-temporal variation in rainfall erosivity during 1960–2012 in the Pearl River basin, China. CATENA 137:382–391

Li J, Wang Z, Wu X et al (2020) Flash droughts in the Pearl River basin, China: observed characteristics and future changes. Sci Total Environ 707:136074

Li J, Wu X, Wang Z et al (2021) Changes of drought characteristics in future in Pearl River Basin describing by a new comprehensive standardized drought index. J Hydraul Eng 52:486–497.

Liu S, Shi H, Niu J et al (2020) Assessing future socioeconomic drought events under a changing climate over the Pearl River basin in south China J Hydrol. Reg Stud 30:100700

Ma X, Yao Y, Zhao Q (2021) Regional GNSS-derived SPCI: verification and improvement in Yunnan, China Remote Sens 13:1918. https://doi.org/10.3390/rs13101918

Mann HB (1945) Nonparametric test against trend. Econometrica 13:245–259

Mckee TB, Doesken NJ, Kleist J (1993) The relationship of drought frequency and duration to time scales. In: Proceedings of the 8th conference on applied climatology, vol 17, p 179–183

Ostad-Ali-Askari K (2022a) Management of risks substances and sustainable development. Appl Water Sci 12:65

Ostad-Ali-Askari K (2022b) Developing an optimal design model of furrow irrigation based on the minimum cost and maximum irrigation efficiency. Appl Water Sci 12:144

Palmer WC (1965) Meteorological drought. US Dep Commer Weather Bur Res Pap 45:1–58

Pei L, Yan Z, Yang H (2015) Multidecadal variability of dry/wet patterns in eastern China and their relationship with the pacific decadal oscillation in the last 413 years. Chin Sci Bull 60:97

Qian W, Hu Q, Zhu Y, Lee DK (2003) Centennial-scale dry-wet variations in east Asia. Clim Dyn 21:77–89

Rabiei J, Khademi MS, Bagherpour S et al (2022) Investigation of fire risk zones using heat-humidity time series data and vegetation. Appl Water Sci 12:216

Schumacher DL, Keune J, van Heerwaarden CC et al (2019) Amplification of mega-heatwaves through heat torrents fuelled by upwind drought. Nat Geosci 12:712

Seo J, Won J, Choi J et al (2022) A copula model to identify the risk of river water temperature stress for meteorological drought. J Environ Manage 311:114861

Vicente-Serrano SM, Begueria S, Lopez-Moreno JI (2010) A multiscalar drought index sensitive to global warming: the standardized precipitation evapotranspiration index. J Clim 23:1696–1718

Wang Y, Shi P, Zeng L et al (2011) Interannual variation of vegetation and precipitation in Pearl River basin during 1982–1999. J Trop Oceanogr 30:44–50

Wang Z, Zhong R, Lai C et al (2018) Climate change enhances the severity and variability of drought in the Pearl River basin in south China in the 21st century. Agric for Meteorol 249:149–162

Wilhite DA (2017) Drought and water crises: integrating science, management, and policy, 2nd edn. CRC Press, Boca Raton

Wu J, Tan X, Chen X, Lin K (2020) Dynamic changes of the dryness/wetness characteristics in the largest river basin of south China and their possible climate driving factors. Atmos Res 232:104685

Xiao M, Zhang Q, Singh VP, Liu L (2016) Transitional properties of droughts and related impacts of climate indices in the Pearl River basin, China. J Hydrol 534:397–406

Xu K, Qin G, Niu J et al (2019) Comparative analysis of meteorological and hydrological drought over the Pearl River basin in southern China. Hydrol Res 50:301–318

Xu WY, Kamide Y (2004) Decomposition of daily geomagnetic variations by using method of natural orthogonal component. J Geophys Res-Space Phys 109:A05218

Wang L, Zhang X, Fang Y et al (2017) AApplicability assessment of China meteorological forcing dataset in upper Yangtze River basin. Water Power 43:18–22

Xie Y, Tu X, Hu Z et al (2020) Evolution of drought levels and impacts of main factors in the Dongjiang River basin. J Nat Disasters 29:69–82

Yang J, Chen H, Hou Y et al (2019) A method to identify the drought-flood transition based on the meteorological drought index. Acta Geographica Sinica 74:2358–2370

Zhang Q, Singh VP, Peng J et al (2012) Spatial-temporal changes of precipitation structure across the Pearl River basin, China. J Hydrol 440:113–122

Zheng Y, Zhang X, Yu J et al (2022) Assessing the joint impact of climatic variables on meteorological drought using machine learning. Front Earth Sci 10:835142

Zhou Z, Shi H, Fu Q et al (2021) Characteristics of propagation from meteorological drought to hydrological drought in the Pearl River basin. J Geophys Res-Atmos 126:e2020JD033959